The use of a glucose-reduced graphene oxide suspension for photothermal cancer therapy

Omid Akhavan[1,2*], Elham Ghaderi[1], Samira Aghayee[1], Yasamin Fereydooni[1], Ali Talebi[1]

[1]Department of Physics, Sharif University of Technology, P.O. Box 11155–9161, Tehran, Iran

[2]Institute for Nanoscience and Nanotechnology, Sharif University of Technology, P.O. Box 14588–89694, Tehran, Iran

* Corresponding author. Tel/Fax: +98–21–66164566. E-mail address: oakhavan@sharif.edu (O. Akhavan)

Abstract

A single-step green method for effective reduction and functionalization of graphene oxide (GO) by glucose was developed. Then, efficacy of the glucose-reduced GO sheets in photothermal therapy of LNCaP prostate cancer cells was investigated in vitro. The GO suspension reduced and functionalized by glucose in presence of Fe catalyst showed a biocompatible property with an excellent near-infrared (NIR) photothermal therapy better than hydrazine-reduced GO, single-wall and multi-wall carbon nanotube suspensions which even showed some levels of toxicities. For complete destruction of the cancer cells under some time intervals of NIR irradiation (e.g., 0.5 and 12 min with power density of 7.5 W/cm^2), minimum concentrations of the reduced GO sheets (i.e., 1 and 0.05 mg/mL) were obtained. The high photothermal therapy efficiency and biocompatibility of the glucose-reduced GO sheets were assigned to functionalization of the reduced sheets by gloconate ions which also prevented their aggregation. Our results suggest that the glucose-reduced GO sheets can be used as biocompatible and efficient photothermal agents in upcoming nanotechnology-based cancer therapies without any common functionalization by polyethylene glycol.

1. Introduction

Although valuable techniques (such as surgery, chemotherapy, radiotherapy, and sometimes a combination of them) have been developed in the area of cancer therapies, there are still important obstacles (e.g., severe adverse reactions [1,2] and low efficiency versus resistant cancer cells [3,4]) which should be resolved. In recent years, photothermal nanotherapy has been proposed for effective treatment of advanced-stage cancer, with low side effects [5–7]. It relies on heat generation in a nanomaterial upon near-infrared (NIR) photoexcitation and destroying cancer cells by excessive local heating.

Graphene (as a monolayer or few layers of sp^2-bonded carbon atoms having a honeycomb lattice structure) with unique physicochemical properties (e.g., see ref. [8]) has attracted much attentions. Furthermore, very similar to carbon nanotubes (CNTs), graphene is capable for absorbing NIR radiation, because of its delocalized electron arrangement. This absorbed radiation can be given off to vibrational modes of the graphene i.e., transformation into thermal energy, which results in raising the temperature of the cancerous tissue and structural changes in the cellular and protein configurations [9]. Hence, graphene sheets with an excellent thermal conductivity [10] and a high effective surface area (as the thinnest sheet) can be considered as one of the most effective nanomaterials in photothermal nanotherapy applications.

So far, only few works about photothermal therapy of cancer cells by graphene-based nanomaterials have been reported. For example, for the first time, Yang *et al.* [11] studied photothermal therapy of cancer cells in-vivo, by using nanoscale graphene oxide (nGO) sheets

coated by polyethylene glycol (PEG). Then, the effect of surface chemistry and size of nanoscale graphene oxide sheets on cancer photothermal therapy using ultra-low laser power was reported by this group [12]. Robinson *et al.* [13] studied photothermal therapy of cancer cells in vitro, by using a low concentration of nanoscale reduced graphene oxide (nRGO)-PEG. Zhang *et al.* [14] reported synergistic effect of chemo photothermal therapy using PEGylated graphene oxide. And Markovic *et al.* [15] found that polyvinylpyrrolidone-coated graphene nanoparticles show better performance in photothermal therapy of cancer cells in vitro than DNA or sodium dodecylbenzenesulfonate-solubilized single-wall carbon nanotubes (SWCNTs). In the most of these recent works, in order to overcome the water-insolubility of hydrazine-reduced graphene oxide sheets, functionalization by PEG was used. In addition, PEG-functionalized nRGO sheets exhibited a biocompatible property, while nGO and nRGO appeared to show similar levels of toxicity [13].

In fact, biocompatibility of graphene-based nanomaterials is one of the most important parameters for their applications in (especially in-vivo) photothermal therapy of cancer cells. Although, there are some investigations about biocompatibility of graphene [16], interaction of extremely sharp edges of graphene sheets with cell wall membrane [17], generation of reactive oxygen species by graphene [18] and trapping a live cell within the aggregated graphene sheets [19] were reported as possible mechanisms for describing the cytotoxicity of graphene sheets. It was also reported that the graphene-based papers can inhibit the growth of bacteria but with a minimal cytotoxicity [20]. Cytotoxicity of graphene is also reported dose dependent [18,21].

Moreover, in the chemical exfoliation method (as one of the most efficient methods for large scale production of graphene), strong reductants such as hydrazine which is highly toxic is usually applied for reduction of the synthesized graphene oxide suspensions. Therefore, not only a biocompatible reductant should be selected and used for reduction of the chemically exfoliated GO suspensions (e.g., melatonin [19,22], vitamin C (L-ascorbic acid) [23], sugar [24], polyphenols of green tea [25] and bacteria [26,27]), but also biocompatibility of the reduced graphene oxide suspension must be tested for a noninvasive and harmless application of graphene-based nanomaterials in photothermal therapy. In addition, lower amounts and concentrations of graphene with higher NIR absorbance and heat transport efficiencies should be prepared and utilized for the photothermal therapy. One of the ways for achieving this purpose is prevention from aggregation of reduced graphene oxide sheets during the biocompatible reduction process at the neutral pH.

In this work, at first, we used glucose for green reduction and functionalization of graphene oxide sheets synthesized through chemical exfoliation method. The efficiency of reduction by glucose in presence of a Fe catalyst was investigated. The biocompatibility of the glucose-reduced graphene oxide was examined and compared to the biocompatibility of hydrazine-reduced graphene oxide, without using any PEGylation which usually applied for functionalization of the reduced sheets. Then, the biocompatible glucose-reduced graphene oxide suspension was used for NIR photothermal therapy of human prostate cancer cells in-vitro. For some various NIR irradiation times, the minimum GO concentration required for complete lysis

of the cancer cells was obtained. Efficiency and biocompatibility of the graphene-based nanomaterials in photothermal therapy were also compared with those of single-wall carbon nanotubes and multi-wall carbon nanotubes (MWCNTs).

2. Experimental Method

2.1. Synthesis of Graphene Oxide (GO)

Natural graphite powder (particle diameter of ≤ 20 μm, Fluka) was utilized as the raw material to prepare graphite oxide suspension through an improved Hummers' method. The details of this method were previously reported elsewhere [22]. The prepared graphite oxide powder was dispersed in deionized (DI) water to obtain an aqueous graphite oxide suspension with yellow-brownish color. The suspension was centrifuged at 2000 rpm for 15 min to eliminate unexfoliated graphitic plates and then at 8000 rpm for 10 min to remove tiny graphite particles. Finally, GO suspension was achieved by exfoliation of the filtered graphite oxide suspension through its sonication at frequency of 40 kHz and power of 150 watt for 1 h

2.2. Reduction of Graphene Oxide by Glucose

To obtain GO suspension reduced by glucose in presence of Fe catalyst (GRGO-Fe), at first, 160 μL glucose solution ($C_6H_{12}O_6$, dextrose 50%) was added to 10 mL of the prepared GO suspension with concentration of 0.1 mg/mL and pH ~7, at room temperature. Then, by using a magneto-stirrer heater, the glucose-GO suspension was stirred at 400 rpm at temperature of 95ºC in presence of a Fe foil with dimensions of 10 mm × 10 mm × 1 mm in air for 30 min. The

glucose-reduced GO (GRGO) suspension was obtained by the same procedure, but without applying the Fe catalyst. To have a better comparison, the efficacy of the glucose solution for reduction of the GO suspension in presence of the Fe catalyst was compared to the efficacies of hydrazine (with concentration of 5 mM) at 90ºC for 10 min. To prevent the fast aggregation of the reduced GO, pH of the hydrazine-reduced GO (HRGO) suspension was adjusted to the range of 9–10 by using ammonia solution (~2 μL for each mL of the suspension).

To compare the photothermal efficiency of our graphene based materials with the efficiency of carbon nanotubes (CNTs), SWCNT (HiPco, with residual Fe catalyst < 35 wt.%, diameter of 0.8–1.2 nm and length of ~100– 1000 nm) and MWCNT (with purity of 95%, outer diameter of 10–30 nm and length of <5–15 μm [28,29], provided from io.li.tec) powders were used. To obtain homogenous suspension, the CNTs were chemically functionalized by sonicating in nitric acid (65%, Merck) at 60–70ºC. Then, the functionalized CNTs were filtered and washed with DI water. Finally, a desired amount of the functionalized CNT powders were dispersed uniformly in DI water.

2.3. Material Characterization

The surface topography and height profile of the GO and reduced-GO layers were studied by using atomic force microscopy (AFM, Digital Instruments NanoScope V) in tapping mode. The coatings for the AFM imaging were prepared by drop–casting a diluted suspension (0.01 mg/mL) onto a cleaned Si(100) substrate. UV-Vis spectrophotometer (Perkin Elmere UV-Vis-NIR Model Lambda 950) was used to investigate the optical absorption of the GO and the

reduced GO suspensions in the wavelength range of 200– 1000 nm. X-ray photoelectron spectroscopy (XPS) was utilized to examine chemical states of the GO layers under the different reducing conditions. The data were obtained through a hemispherical analyzer equipped by an Al Kα X-ray source (hν = 1486.6 eV) operating at a vacuum $<10^{-7}$ Pa. The XPS peaks were deconvolution by using Gaussian components after a Shirley background subtraction. To study the carbon structure of the samples, Raman spectroscopy (HR-800 Jobin -Yvon) equipped by an Nd-YAG laser source operating at wavelength of 532 nm was applied at room temperature .

2.4. Cell Culture and Cellular Incubation in Graphene-based Suspension

The human prostate cancer cell line LNCaP (ATCC, Rockville, MD) was cultured in RPMI-1640 medium (ATCC, Rockville, MD) supplemented with 10% fetal bovine serum (FBS) and 1% penicillin-streptomycin. Then, the cancer cells were incubated within a 100 mL flask containing ~2×10^6 cells and 200 μL reduced GO suspension (with various concentrations of GO ranging from 0.001 to 1 mg/mL) for 24 h at 37°C in a 5% CO_2 atmosphere. As an advantage, no significant aggregation was observed for the GRGO and GRGO-Fe added to the culture medium, while the GO suspension showed a slight instability in the culture medium.

2.5. Photothermal Therapy and Determination of Live Cells

For NIR photothermal therapy, the cancer cells incubated in the graphene-based suspension were transferred to a cubical quartz cuvette (with dimension of 2 cm) and exposed to an 808 nm diode laser source (JENOPTIK unique-mode GmbH, Germany) with the beam diameter of about 1 cm and power density of 7.5 W/cm^2. After the photothermal process, the

number of live cells was determined using a 3-(4,5-dimethylthiazol-2-yl)-2,5-diphenyltetrazolium bromide (MTT) cell proliferation assay kit. The data reported in this work are average of three measurements. To have some optical images from the photothermal destruction of the cells, multiple regions of the GRGO-incubated cancer cells cultured on a plate were exposed to the NIR laser irradiation for various periods of time and then stained with 1% Trypan Blue for 15 min to check the cell viability. A dead cell absorbs the dye and shows a blue color cell, while a living cell eliminates the dye and stays transparent.

2.6. Measurement of Heating of the Graphene-Based Suspensions by NIR Irradiation

The graphene-based suspensions were heated under irradiation by the NIR laser. Temperature of the suspensions was measured at 15-s intervals with a thermocouple located inside the suspension for a total time of 2 min. In order to minimize the direct heating, exposure of the thermocouple by the laser beam was prevented.

3. Results and discussion

Figure 1a presents AFM image of the GO sheets deposited on the Si substrate. Three overlapped sheets are observable in the image. The height profile diagram of the AFM image indicates that the thickness of the sheets is around 1 nm, comparable to the typical thickness of the single-layer GO sheets (~0.8 nm) [30,31]. Figure 1b shows the GO sheets reduced by hydrazine with average thickness of ~0.55 nm. In fact, removing the epoxy and hydroxyl groups from the both sides of GO sheets results in ~0.44 nm decrease for approaching to the thickness of graphene (~0.36 nm)

[32]. Figure 1c exhibits the GO sheets reduced by glucose in presence of Fe catalyst with average thickness of ~1.4 nm. The increase in thickness of the reduced sheets (~1 nm) can be assigned to adsorption of reductant molecules (here, glucose-based molecules) on the both sides of the reduced sheets, as reported by Su *et al.* [33], but for some aromatic molecules. Then, the remained thickness of about 0.4 nm can be attributed to thickness of the reduced GO sheets, as similarly reported for GO sheets reduced by vitamin C [23] and melatonin [22].

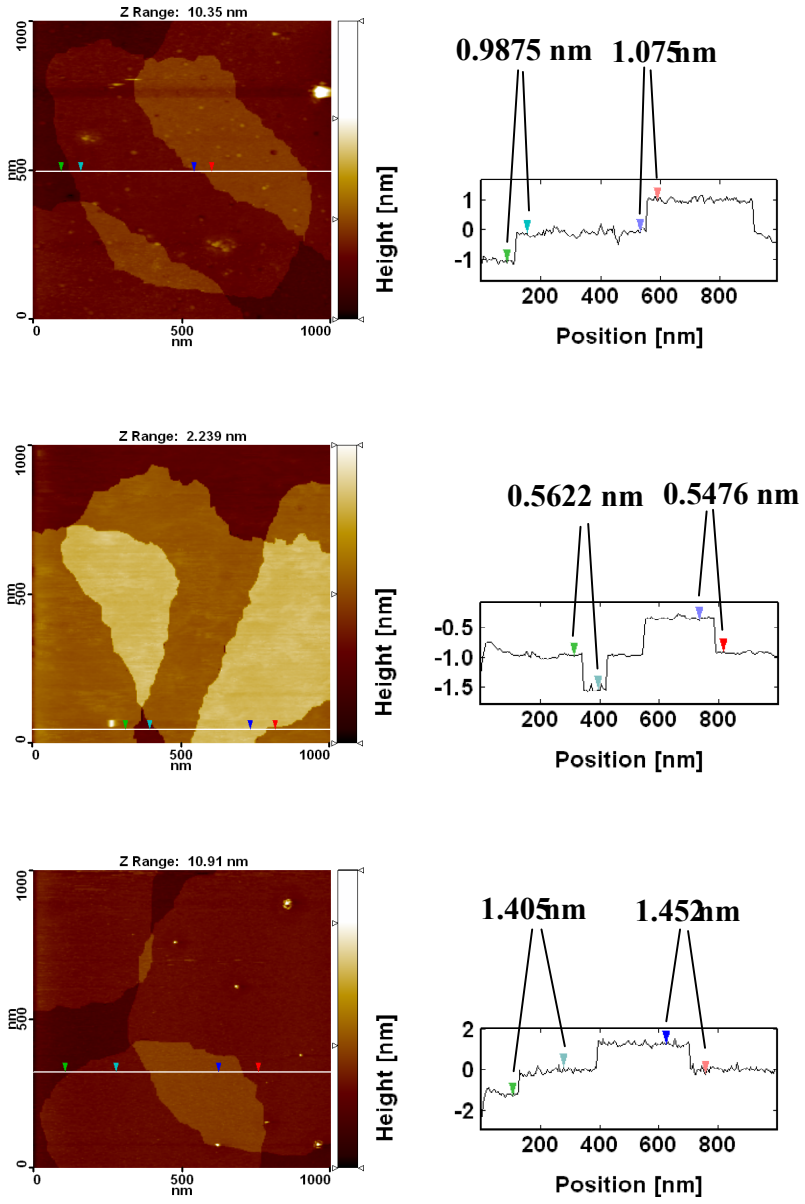

Figure 1. AFM images of a) the GO nanosheets and the GO nanosheets reduced by b) hydrazine at 90 ºC for 10 min and c) glucose in presence of a Fe foil catalyst at 95ºC for 30 min. Vertical distances of the markers were noted above the height profile diagrams.

The optical absorption spectra of the GO and reduced GO suspensions are exhibited in Figure 2. After reduction of the GO by either glucose or hydrazine, color of the GO suspension changed from light brown to black (see the inset of Figure 2). The black color of the reduced GO suspensions can be assigned to partial restoration of the π network between the sheets due to removing the oxygen-containing bonds resulted in electronic conjugation within reduced sheets [34]. The optical absorption spectra also show that the absorption peak of the GO suspension is around 228 nm, while the absorption peaks of the reduced suspensions shift into wavelengths of around 265 nm, corresponding to deoxygenation of the GO suspension under the reduction processes. It is also seen that the absorption around wavelength of 800nm significantly increased by reduction of the GO suspension. The GO reduced by hydrazine and glucose in presence of Fe showed the highest optical absorption among the samples. The lower optical absorption of the GRGO sample can be assigned to incomplete reduction of the GRGO as compared to the reduction of the HRGO and GRGO-Fe suspensions.

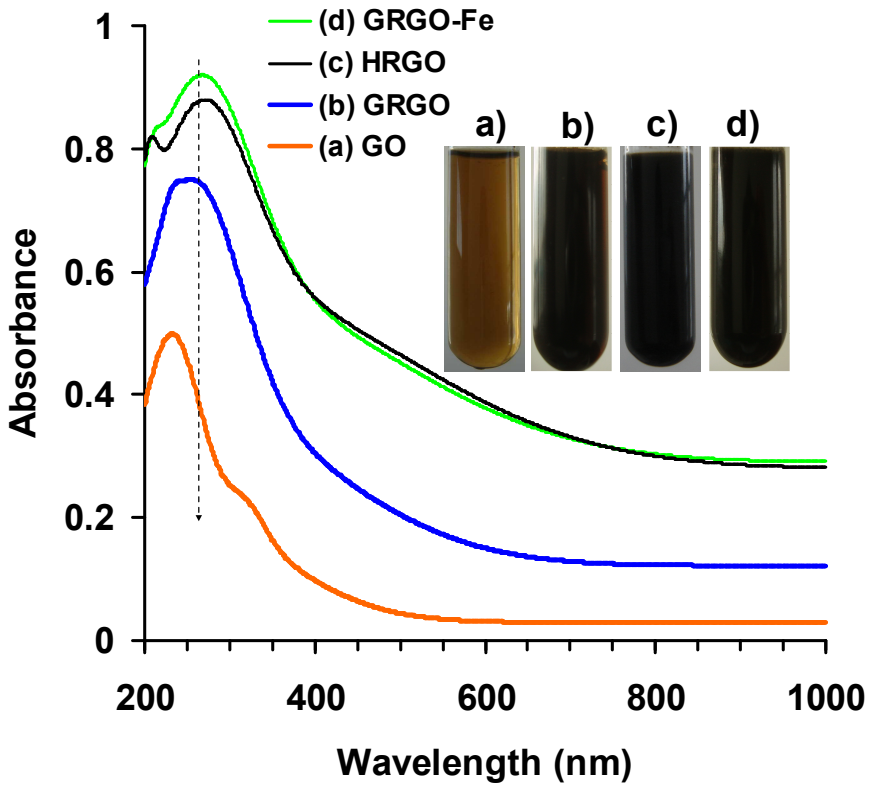

Figure 2. UV-vis absorption spectra of a) GO, b) GRGO, c) HRGO, and d) GRGO-Fe suspensions with GO concentration of 0.5 mg/mL. Inset shows digital pictures of the reduced GO suspensions (b–d) as compared to the as-prepared GO suspension (a).

To study the effect of glucose on the deoxygenation of the GO suspension in more details, XPS was used. Figure 3 shows deconvoluted C(1s) peaks of the GO reduced by glucose in absence and in presence of Fe catalyst, as compared to the peaks of the as-prepared GO and the HRGO. The deconvoluted peak centered at 285.0 eV was attributed to the C–C and C=C

bonds. The other peaks located at the binding energies of 286.5, 287.2, 288.2 and 289.4 eV were attributed to the C–OH, C–O–C, C=O, and O=C–OH oxygen-containing functional groups, respectively (see, e.g., Refs. [35,36]). In order to quantitatively investigate the chemical states of the GO sheets at the various reduction conditions, the peak area ratios of the C–OH, C–O–C, C=O and O=C–OH peaks to the CC peak were extracted from the deconvoluted peaks, as given in Table 1. It was found that, glucose is able to partially reduce the GO (compare Figure 3a and 3b), but the reduction level of the GO by glucose in presence of the Fe catalyst (Figure 3d) was comparable to the reduction level achieved by hydrazine (Figure 3e), except that the XPS of the HRGO indicated another peak component at 286.0 eV relating to formation of C –N bond (see, for example, Ref. [22]). In addition, although no peak relating to formation of the C–N bond was observed in the XPS of the GO reduced by glucose, but the XPS peak of the GRGO-Fe exhibited a significant deconvoluted peak relating to epoxide groups. Presence of epoxide groups in the reduced sample was assigned to functionalization of the reduced sheets through formation of a chemical bond between the gluconate ions and the carbons of the reduced GO, as discussed further in the following. The quantitative variations in the chemical state of the GO after the reduction processes are given in Table 1. It is worthy to note that the Fe(2p) core level of the Fe catalyst before use in the reduction process was consistent with Fe^0 chemical state and no significant change was observed after the reduction process by glucose. This confirmed that the Fe foil did not oxidize and acted as a catalyst during the reduction process.

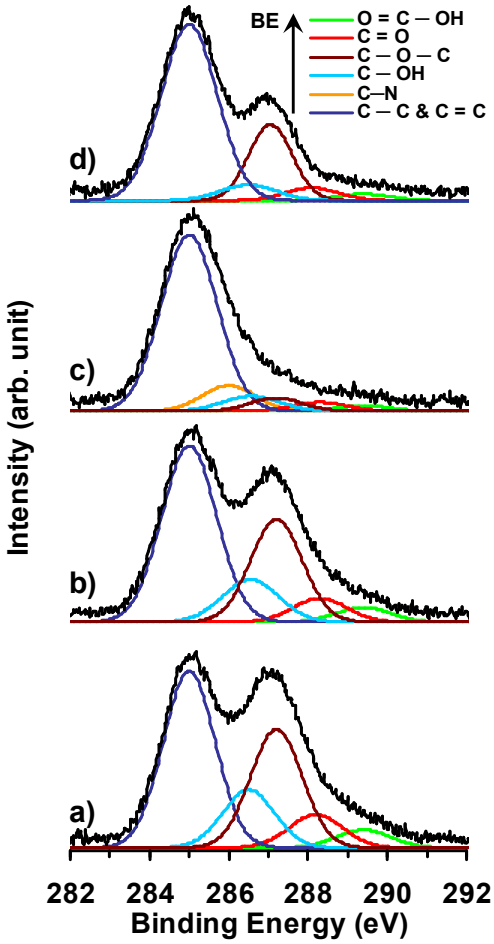

Figure 3. Peak deconvolution of C(1s) core level of XPS spectra of a) GO, b) GRGO, c) HRGO, and d) GRGO-Fe.

Raman spectroscopy is known as an effective technique for investigation on the single- and multi-layer properties of graphene sheets. Here, the effects of the various reduction conditions on the Raman characteristics of the reduced GO sheets were examined, as shown in Figure 4. The famous properties of carbon materials in Raman spectra are the G band (~1580

cm^{-1}) originated from the phonon scattering of the graphitic structure and the D band (~1350 cm^{-1}) relating to formation of sp^3 defect bonds caused by oxidation [37,38]. In addition, the D band can be resulted from vacancies, grain boundaries, edge defects and amorphous carbon species in a disordered carbon structure [39]. In this regard, the I_G/I_D ratio is defined as a parameter for measuring the sp^2 domain size of a carbon structure containing sp^3 and sp^2 bonds. In this work, for the GO suspensions reduced at the different conditions, the I_D/I_G ratios (inverse of I_G/I_D) were given in Table 1. It was found that deoxygenation of the GO sheets by using glucose solution in presence of the Fe catalyst resulted in reduction of the I_D/I_G ratio which can be attributed to recovering the graphitic structure of the GO sheets during the reduction. However, for the HRGO the I_D/I_G ratio was found about 1.37 which can be assigned to increase of the defects on surface of the reduced GO through formation of the C–N bonds.

Raman spectra of graphene-based materials also shows a 2D band (described by the adopted double resonant model [39,40]) which is sensitive to stacking of graphene sheets [41]. For single-layer graphene sheets, the 2D band generally appears as a Lorentzian peak centered at 2679 cm^{-1}, while for multilayer graphene sheets (including 2–4 layers) the 2D band shows a wider peak with 19 cm^{-1} shift to higher wavenumbers [42]. Figure 4 shows that the 2D band of the as-prepared GO sheets centered about 2686 cm^{-1} with a low-intensity shoulder at the higher wavenumbers. Hence, monolayer GO sheets were present in the as-prepared GO suspension. Although, the 2D bands of the HRGO exhibited a significant shift into the higher wavenumbers, the 2D band of the GRGO-Fe showed only a slight shift indicating lower aggregation of the GO

sheets reduced by glucose in presence of the Fe catalyst. The lower aggregation in the GRGO-Fe suspension can be assigned to adsorption of the gluconate ions on the reduced sheets, consistent with the results obtained by the XPS analysis. Furthermore, the peak appeared at ~1130 cm^{-1} confirmed attachment of glucose and/or glucose oxide molecules on surface of the GRGO-Fe sheets (see Figure 4d). On the other hand, the lower aggregation in the GRGO suspension (as resulted from the lower shift in the 2D band) can be assigned to its lower reduction level. Meanwhile, the Raman spectrum (Figure 4b) shows lower amounts of glucose and/or glucose oxide molecules on surface of the GRGO sheets.

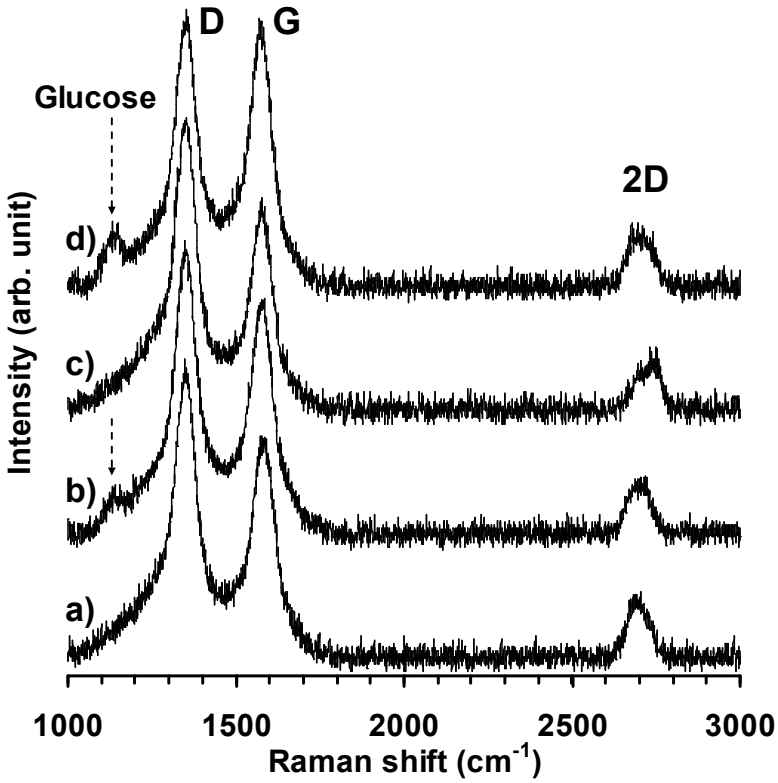

Figure 4. Raman spectra of a) GO, b) GRGO, c) HRGO, and d) GRGO-Fe.

Table 1. The peak area (A) ratios of the oxygen-containing bonds to the CC bonds and the peak intensity ratio of I_D/I_G of the GO reduced in the various conditions.

Samples		GO	GO reduced by		
			Glucose	Hydrazine	Glucose-Fe
XPS	A_{CN}/A_{CC}	–	–	0.14	–
	A_{COH}/A_{CC}	0.33	0.25	0.08	0.09
	A_{COC}/A_{CC}	0.67	0.55	0.07	0.33
	A_{CO}/A_{CC}	0.19	0.13	0.05	0.07
	A_{OCOH}/A_{CC}	0.11	0.08	–	0.04
Raman	I_D/I_G	1.22	1.18	1.37	0.97

It was shown that metallic particles such as Au, Pt and Pd [36] and metal oxides such as TiO_2 [43–45], ZnO [46–48] and WO_3 [49,50] can play a (photo)catalytic role in reduction of graphene oxide, through electron transferring from (photo)catalysts into graphene oxide. Here, the Fe foil can play the same role as catalyst and contribute in the electron transferring into the GO based on the following reactions:

$Fe \rightarrow Fe^{2+} + 2e^-$

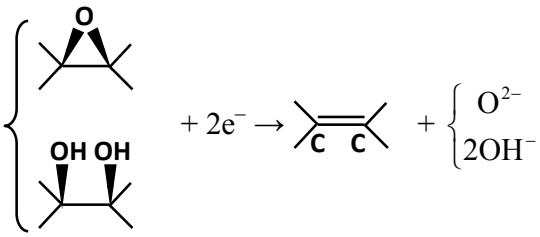

in which the upper and lower symbols show epoxide and hydroxide of GO, respectively. Now, the Fe^{2+} can promote oxidizing the glucose in presence of oxygen dissolved in the aqueous solution as shown in the following [51]:

Glucose ($C_6H_{12}O_6$) + H_2O + Fe^{2+} → Gluconicacid ($C_6H_{12}O_7$) + Fe + $2H^+$

Then, the glucose oxidizing results in reduction of GO as follows:

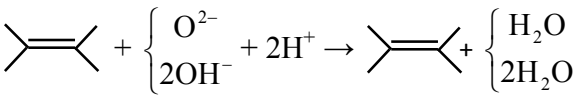

In addition, glucose and gluconicacid can chemically bond to carbon of GO as schematically shown in Figure 5 for glucose. This bonding is similar to chemical bonding of glucose to phosphate groups through phosphorylation of glucose which was previously reported by others (see, for example, Ref. [52]) The steric effect of this chemical bonding (which formation of its

C–O–C bond on surface of the reduced GO sheet was confirmed by the XPS analysis of the GRGO-Fe) resulted in low aggregation of the reduced GO sheets, as also found by Raman analysis.

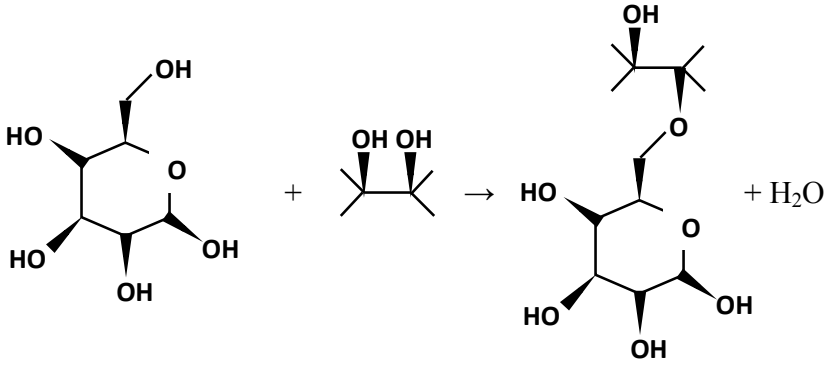

Figure 5. Schematic reaction of glucose and hydroxyl bonds of GO.

The GRGO-Fe sheets which obtained by using a green reaction were utilized for destruction of LNCaP prostate cancer cells through a photothermal therapy. After the therapy, cell viability of the cancer cells was detected by MTT test. The photothermal effects of GRGO-Fe and also other graphene-based materials (i.e., GO, GRGO, and HRGO) on the therapy of the cancer cells were investigated and compared to the corresponding effects of the oxidized SWCNT and MWCNT powders as benchmarks for carbon nanomaterials. Concerning this, Figure 6a shows that by using GRGO-Fe, HRGO, SWCNT and MWCNT suspensions most of the cancer cells (~93, 87, 91 and 70%) died just after 1 min, while using the GRGO only ~18% of the cells were destructed at the same irradiation time. The GO suspension was transparent and

so no significant cancer cell destruction was observed, very similar to the control sample with no carbon nanomaterials.

Because a portion of the observed cell destruction can be assigned to cytotoxicity of the carbon nanomaterials, we also checked MTT cytotoxicity of our carbon-based nanomaterials in dark, as shown in Figure 6a. It was found that, although the GO and GRGO suspensions were biocompatible, the HRGO suspension indicated a cytotoxic property against the prostate cancer cell. It was found that by removing the residual hydrazine of the suspension through filtration and then adjusting pH of the final suspension to ~7, a nearly biocompatible but aggregated reduced GO suspension obtained. Therefore, the cytotoxicity of the HRGO suspension can be assigned to the residual hydrazine of the suspension (as known as a toxic material), high pH (>7) of the suspension and/or the cytotoxicity of the non-aggregated reduced GO sheets with extremely sharp edges, as previously reported elsewhere [17]. Strong cytotoxicity of the oxidized SWCNTs and partial cytotoxicity of the oxidized MWCNTs against the prostate cancer cells were also observed, in consistent with some previous reports for cytotoxicity of these carbon-based nanomaterials against various human and animal cells [53−56] and bacteria [57−59]. In contrast to these toxic carbon-based nanomaterial suspensions, the GRGO-Fe showed a biocompatible property which can be assigned to the biocompatible pH of the suspension (~7), absence of any residual toxic agents required in synthesis of the non-aggregated reduced GO sheets, and/or the steric effect of gluconate ions attached on the reduced sheets prevented effective direct contact interaction of the sheets with wall membrane of the cells. Although the

GRGO-Fe, the HRGO and the functionalized SWCNT suspensions exhibited nearly the same efficiencies for the photothermal therapy, biocompatible property of the GRGO-Fe indicates its more effective performance in the photothermal therapy than the performance of the cytotoxic HRGO and SWCNT suspensions (because some portion of the cell destruction can be assigned to the cytotoxic property of the carbon materials, not to the photothermal therapy). Since the level of reduction of the GRGO-Fe and HRGO is the same (see Table 1), the better performance of the GRGO-Fe than the HRGO can be assigned to lower aggregation of the reduced sheets in the GRGO-Fe (as shown by Raman), providing more effective surface area for further NIR absorption and better heat transferring to the cells. Therefore, the GRGO-Fe can be nominated as a biocompatible graphene-based nanomaterial for efficient photothermal therapy of cancer cells.

Since the cell death following exposure of carbon nanomaterials to NIR radiation can be assigned to thermal disintegration, temperature of the different solutions (including the solutions containing GO, GRGO-Fe, HRGO and a control sample without any carbon nanomaterials) was measured, as shown in Figure 6b. The control sample (a solution without any carbon nanomaterials) was transparent to the NIR irradiation and so negligible heating was detected. Similarly, the transparency of the GO solution resulted in only a little heating of the solution after 2 min NIR irradiation, as can be seen in Figure 6b. However, the NIR irradiation of the aqueous solutions containing GRGO-Fe, HRGO with GO concentration of 0.1mg /mL for 2 min caused heating of the solution to temperatures of about 64 and 70°C, respectively. For longer irradiations, boiling of the solutions was also observed. These results indicated that the energy

absorbed by the photo-stimulated graphene-based nanomaterials can quickly transfer to molecular vibration energies and consequently heating. It should be noted that, the biocompatible GRGO-Fe solution with a slight lower temperature (64°C) was more efficient than the toxic HRGO with higher temperature (70°C) in photothermal destruction of the cancer cells. This means that the photo-stimulated GRGO-Fe showed a better heat transfer to the cancer cells (rather than the solution), and consequently, a further increase in local temperature of the cells (as compared to the measured temperature of the solution) than the photo-stimulated HRGO. The better heat transfer of the GRGO-Fe than the HRGO can be assigned to higher content of single-sheets of reduced graphene in the former, as also found by analysis of the Raman spectra.

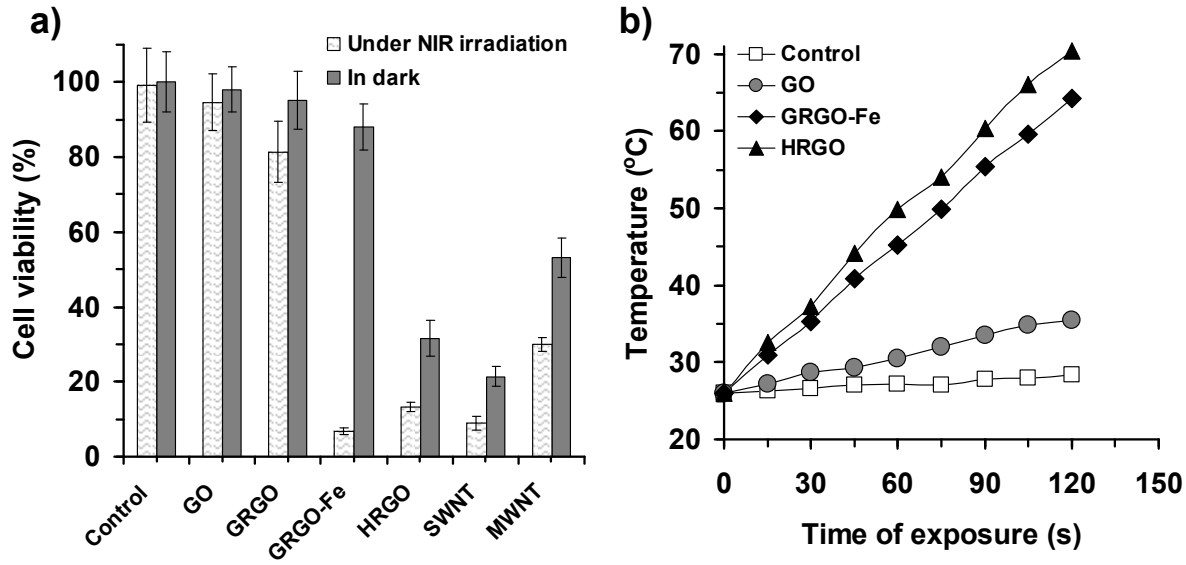

Figure 6. a) Cell viability of LNCaP prostate cancer cells after exposing to the GO suspension and the GRGO, GRGO-Fe, and HRGO with GO concentration of 0.1 mg/mL, as compared to the same concentration for the oxidized SWCNTs and MWCNTs, under irradiation of an 808-nm laser source with power density of 7.5 W/cm^2 for 1 min and in dark for 24 h. Control sample shows the cell viability in a solution without any GO additive. b) Temperature evolution of the cancer cell solution containing 0.1 mg/mL of the GO, GRGO-Fe and HRGO during continuous irradiation by the laser source for 2 min.

The cell viability of the cancer cells was studied by using bright-field inverted microscopy method (Figure 7) and MTT test (Figure 8a), after photothermal therapy by the GRGO-Fe at various NIR irradiation times. For the microscopy method, the cells were stained with Trypan Blue to find the extent of the cell death. The circular regions in Figure 7 represent

the position of laser spots. Radius of the laser spot was ~5 mm, as measured by using a photosensitive paper. A control sample was also incubated without any graphene-based nanomaterials (see the right column in Figure 7). The left column in Figure 7 shows that mortal cells appeared after 30 s photothermal therapy. By increasing the irradiation time to 120 s, most of the cancer cells, especially located at center of the circular area, were dead. The same results were obtained by MTT test as shown in Figure 8a. The control samples showed no considerable mortal cells even after 120 s NIR irradiation (see Figure 7 and 8a). Figure 7 also shows that no considerable dead cells were distinguishable for the cells outside of the laser spot, very similar to the control samples. This means that the GRGO-Fe sheets themselves showed no significant cytotoxic property. The MTT test also indicated that that the transparent GO sheets were not so effective in the photothermal therapy (see Figure 8a). This presents the effect of the effective deoxygenation of GO through reduction by glucose in presence Fe catalyst on the photothermal therapy of the cells.

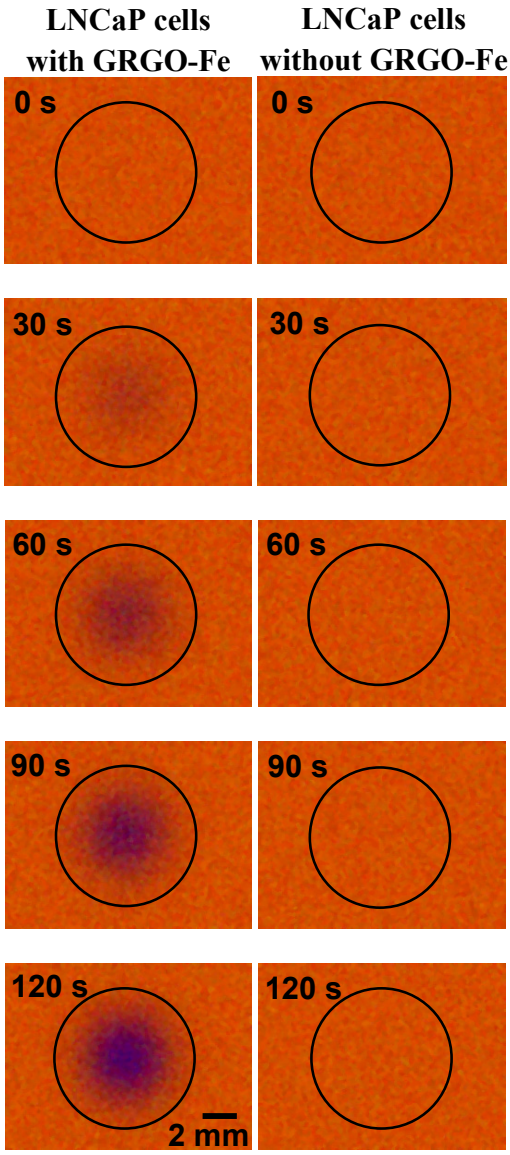

Figure 7. Optical images of photothermal destruction of LNCaP prostate cancer cells incubated with 0.05 mg/mL GRGO-Fe nanosheets at various times of NIR irradiation with power density of 7.5W /cm^2. The circles show position of the laser spot.

Using MTT test, we also studied the effect of various concentrations of GRGO-Fe on the photothermal therapy of the cancer cells for different NIR irradiation times, as shown in Figure 8b. It was found that for the high concentration of 1 mg/mL, only 0.5min irradiation time was required for photothermal destruction of whole of the cancer cells. On the other hand, the lowest concentration required for complete photothermal lysis of the cancer cells within the long irradiation time of 12 min was 0.05 mg/mL. To have some comparison, it is worthy to note that, Yang *et al.* [11] could completely eliminate the tumors of mice through intravenously injection of 2 mg/mL nGO-PEG after 24 h NIR irradiation with power density of 2 W/cm^2. This group using nRGO-PEG (2 mg/mL) obtained a completely tumor elimination by using ultra-low power density of 0.15 W/cm^2 for 5 min [12]. Robinson *et al.* [13] could photothermally destruct 80% of cancer cells in vitro, by using low-concentration (6.6 mg/L) of nRGO-PEG after 20 min NIR irradiation with power density of 15.3 W/cm^2. Therefore, the efficiency of the GRGO-Fe sheets in the photothermal nanotherapy is comparable with the efficiencies have been reported so far.

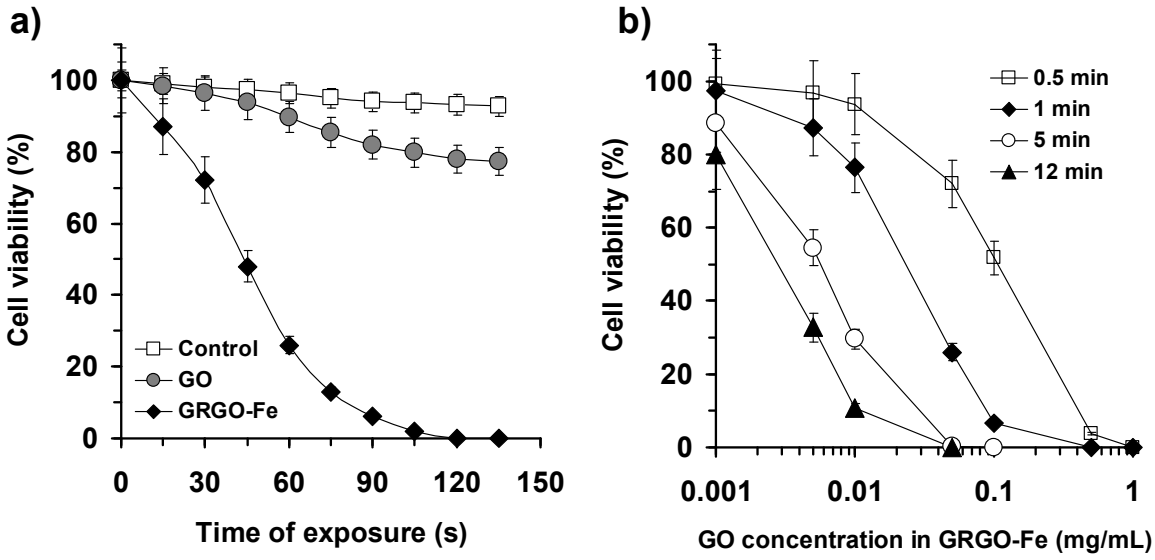

Figure 8. Cell viability of LNCaP prostate cancer cells versus a) NIR irradiation exposure time after incubation with the GO and the GRGO-Fe (with GO concentration of 0.05 mg/mL) as compared to a control sample (cancer cells without the graphene materials) and b) GO concentration in the GRGO-Fe at some various NIR irradiation exposure times.

4. Conclusions

Biocompatible reduced graphene oxide sheets with suitable water-solubility were obtained through functionalization of the reduced sheets by gloconate ions produced during the reduction by glucose in the presence of Fe catalyst, without any PEGylation (as a common functionalization method). In addition, for the first time, the GRGO-Fe was utilized as a biocompatible graphene-based nanomaterial suspension for a high efficient NIR photothermal therapy of LNCaP prostate cancer cells in vitro. It was found that, the GRGO-Fe with high (low)

concentration of 1 (0.05) mg/mL requires only 0.5(12) min for complete destruction of the cancer cells under irradiation of an 808-nm laser source with power density of 7.5 W/cm^2. Although the photothermal therapy using the HRGO, SWCNT and MWCNT suspensions could show similar efficiencies, but these suspensions indicated some cytotoxic effects. These results indicated that the GRGO-Fe can be nominated as one of the promising biocompatible nanomaterials for application in effective NIR photothermal nanotherapy of cancer cells.

Acknowledgements. O. Akhavan would like to thank the Research Council of Sharif University of Technology and also Iran Nanotechnology Initiative Council for financial support of the work.

References:

[1] Coates A, Abraham S, Kaye SB, Sowerbutts T, Frewin C, Fox RM, Tattersall, H. On the receiving end-patient perception of the side-effects of cancer chemotherapy. Eur J Cancer Clin Oncol 1983;19:203–208.

[2] Zachariah B, Balducci L, Venkattaramanabalaji GV, Casey L, Greenberg HM, DelRegato JA. Radiotherapy for cancer patients aged 80 and older: a study of effectiveness and side effects. Int J Radiat Oncol Biol Phys 1997;39:1125–1129.

[3] Michael MG, Tito F, Susan EB. Multidrug resistance in cancer: role of ATP-dependent transporters. Nat Rev Cancer 2002;2:48–58.

[4] Szakács G, Paterson JK, Ludwig JA, Booth-Genthe C, Gottesman MM. Targeting multidrug resistance in cancer. Nat Rev Drug Discovery 2006;5:219–34.

[5] Moon HK, Lee SH, Choi HC. In vivo near-infrared mediated tumor destruction by photothermal effect of carbon nanotubes. ACS Nano 2009;3:3707–3713.

[6] Zhou F, Xing D, Ou Z, Wu B. Cancer cell photothermal therapy in near infrared region by using single walled carbon nanotubes. J Biomed Opt 2009;142:021009.

[7] Ghosh S, Dutta S, Gomes E, Carroll D, D'Agostino Jr R, Olson J, Gmeiner WH. Increased heating efficiency and selective thermal ablation of malignant tissue with DNA-encased multiwalled carbon nanotubes. ACS Nano 2009;3:2667–2673.

[8] Akhavan O, Ghaderi E, Rahighi R. Towards single-DNA electrochemical biosensing by graphene nanowalls. ACS Nano. DOI: 10.1021/nn300261t.

[9] Leper DB. Molecular and cellular mechanisms of hyperthermia alone or combined with other modalities. in: hyperthermic oncology. Overgaard J. ed., (London: Taylor and Francis, 1984), pp. 9–40.

[10] Koh YK, Bae M, Cahill DG, Pop E. Heat conduction across monolayer and few-layer graphenes. Nano Lett2010 ;10:4363–4368.

[11] Yang K, Zhang S, Zhang G, Sun X, Lee ST, Liu Z. Graphene in Mice: Ultrahigh in vivo tumor uptake and efficient photothermal therapy. Nano Lett 2010;10:3318–3323.

[12] Yang K, Wan J, Zhang S, Tian B, Zhang Y, Liu Z. The influence of surface chemistry and size of nanoscale graphene oxide on photothermal therapy of cancer using ultra-low laser power. Biomaterials 2011;33:2206–2214

[13] Robinson JT, Tabakman SM, Liang Y, Wang H, Sanchez Casalongue H, Vinh D, Dai, H. Ultrasmall reduced graphene oxide with high near-infrared absorbance for photothermal therapy. J Am Chem Soc 2011;133:6825–6831.

[14] Zhang W, Guo Z, Huang D, Liu Z, Guo X, Zhong H. Synergistic effect of chemo-photothermal therapy using PEGylated graphene oxide. Biomaterials 2011;32:8555–8561.

[15] Markovic ZM, Harhaji-Trajkovic LM, Todorovic-Markovic BM, Kepic DP, Arsikin KM, Jovanovic SP, Pantovic AC, Dramicanin MD, Trajkovic VS. In vitro comparison of the

photothermal anticancer activity of graphene nanoparticles and carbon nanotubes. Biomaterials 2011;32:1121–1129.

[16] Park S, Mohanty N, Suk JW, Nagaraja A, An J, Piner RD, Cai W, Dreyer DR, Berry V, Ruoff RS. Biocompatible, robust free-standing paper composed of a TWEEN/graphene composite. Adv Mater 2010;22:1736–1740.

[17] Akhavan O, Ghaderi E. Toxicity of graphene and graphene oxide nanowalls against bacteria. ACS Nano 2010;4:5731–5736.

[18] Zhang Y, Ali SF, Dervishi E, Xu Y, Li Z, Casciano D, Biris AS. Cytotoxicity effects of graphene and single-wall carbon nanotubes in neural phaeochromocytoma-derived PC12 cells. ACS Nano 2010;4:3181–3186.

[19] Akhavan O, Ghaderi E, Esfandiar A. Wrapping bacteria by graphene nanosheets for isolation from environment, reactivation by sonication and inactivation by near-infrared irradiation. J Phys Chem B 2011;115:6279–6288.

[20] Hu W, Peng C, Luo W, Lv M, Li X, Li D, Huang Q, Fan C. Graphene-based antibacterial paper. ACS Nano 2010;4:4317–4323.

[21] Liao KH, Lin YS, MacOsko CW, Haynes CL. Cytotoxicity of graphene oxide and graphene in human erythrocytes and skin fibroblasts. ACS Appl Mater Interfaces 2011;3:2607–2615.

[22] Esfandiar A, Akhavan O, Irajizad. A. Melatonin as a powerful bio-antioxidant for reduction of graphene oxide. J Mater Chem 2011;21:10907–10914.

[23] Gao J, Liu F, Liu Y, Ma N, Wang Z, Zhang X. Environment-friendly method to produce graphene that employs vitamin C and amino acid. Chem Mater 2010;22:2213–2218.

[24] Zhu C, Guo S, Fang Y, Dong S. Reducing Sugar: New functional molecules for the green synthesis of graphene nanosheets. ACS Nano 2010;4:2429–2437.

[25] Akhavan O, Kalaee M, Alavi ZS, Ghiasi SMA, Esfandiar A. Increasing the antioxidant activity of green tea polyphenols in the presence of iron for the reduction of graphene oxide. Carbon 2012, 50, 3015–3025.

[26] Akhavan O, Ghaderi E. *Escherichia coli* bacteria reduce graphene oxide to bactericidal graphene in a self-limiting manner. Carbon 2010;50:1853–1860.

[27] Salas EC, Sun Z, Lüttge A, Tour JM. Reduction of Graphene Oxide via Bacterial Respiration. ACS Nano 2010;4:4852–4856.

[28] Akhavan O, Azimirad R, Safa S, Larijani MM. Visible light photo-induced antibacterial activity of CNT-doped TiO_2 thin films with various CNT contents. J Mater Chem 2010;20:7386–7392.

[29] Akhavan O, Azimirad R, Safa S. Functionalized carbon nanotubes in ZnO thin films for photoinactivation of bacteria. Mater Chem Phys 2011;130:598–602.

[30] Schniepp HC, Li JL, McAllister MJ, Sai H, Herrera-Alonso M, Adamson DH, Prud'homme RK, Car R, Saville DA, Aksay IA. Functionalized single graphene sheets derived from splitting graphite oxide. J Phys Chem B 2006;110:8535–8539.

[31] Akhavan O. The effect of heat treatment on formation of graphene thin films from graphene oxide nanosheets. Carbon 2010;48:509–519.

[32] McAllister MJ, Li JL, Adamson DH, Schniepp HC, Abdala AA, Liu J, Herrera-Alonso M, Milius DL, Car R, Prud'homme RK, Aksay IA. Single sheet functionalized graphene by oxidation and thermal expansion of graphite. Chem Mater 2007;19:4396–4404.

[33] Su Q, Pang S, Alijani V, Li C, Feng X, M€ullen K. Composites of graphene with large aromatic molecules. Adv Mater 2009;21:3191–3195.

[34] Li D, Muller MB, Gilje S, Kaner RB, Wallace GG. Processable aqueous dispersions of graphene nanosheets. Nature Nanotechnol 2008;3:101–105.

[35] Liu F, Seo TS. A controllable self-assembly method for large-scale synthesis of graphene sponges and free-standing graphene films. Adv Funct Mater 2010;20:1–7.

[36] Xu C, Wang X, Zhu J. Graphene-metal particle nanocomposites. J Phys Chem C 2008;112:19841–19845.

[37] Ferrari AC, Robertson J. Interpretation of Raman spectra of disordered and amorphous carbon. J Phys Rev B 2000;61:14095–14107.

[38] Stankovich S, Dikin DA, Piner RD, Kohlhaas KA, Kleinhammes A, Jia Y, Nguyen ST, Ruoff RS. Synthesis of graphene-based nanosheets via chemical reduction of exfoliated graphite oxide. Carbon 2007;45:1558–1565.

[39] Ferrari AC, Meyer JC, Scardaci V, Casiraghi C, Lazzeri M, Mauri F, Piscanec S, Jiang D, Novoselov KS, Roth S, Geim AK. Raman spectrum of graphene and graphene layers. Phys Rev Lett 2006;97:187401–187405.

[40] Thomsen C, Reich S. Double resonant Raman scattering in graphite. Phys Rev Lett 2000;85:5214–5217.

[41] Malard LM, Pimenta MA, Dresselhaus G, Dresselhaus MS. Raman spectroscopy in graphene. Phys Rep 2009;473:51–87.

[42] Graf D, Molitor F, Ensslin K, Stampfer C, Jungen A, Hierold C, Wirtz, L. Spatially resolved Raman spectroscopy of single- and few-layer graphene. Nano Lett 2007;7:238–242.

[43] Akhavan O, Ghaderi E. Photocatalytic reduction of graphene oxide nanosheets on TiO_2 thin film for photoinactivation of bacteria in solar light irradiation. J Phys Chem C 2009;113:20214–20220.

[44] Williams G, Seger B, Kamat PV. TiO_2-graphene nanocomposites. UV-assisted photocatalytic reduction of graphene oxide. ACS Nano 2008;2:1487–1491.

[45] Akhavan O, Abdolahad M, Esfandiar A, Mohatashamifar M. Photodegradation of graphene oxide sheets by TiO_2 nanoparticles after a photocatalytic reduction. J Phys Chem C 2010;114:12955–12959.

[46] Akhavan O. Graphene nanomesh by ZnO nanorod photocatalysts. ACS Nano 2010;4:4174–4180.

[47] Williams G, Kamat PV. Graphene-semiconductor nanocomposites: excited-state interactions between ZnO nanoparticles and graphene oxide. Langmuir 2009;25:13869–13873.

[48] Akhavan O. Photocatalytic reduction of graphene oxides hybridized by ZnO nanoparticles in ethanol. Carbon 2011;49:11–18.

[49] Ng YH, Iwase A, Bell NJ, Kudo A, Amal R. Semiconductor/reduced graphene oxide nanocomposites derived from photocatalytic reactions Catal Today 2011;164:353–357.

[50] Akhavan O, Choobtashani M, Ghaderi E. Protein degradation and RNA efflux of viruses photocatalyzed by graphene-tungsten oxide composite under visible light irradiation. J Phys Chem C, DOI: 10.1021/jp301707m.

[51] Zeng Q, Cheng JS, Liu XF, Bai HT, Jiang JH. Palladium nanoparticle/chitosan-grafted graphene nanocomposites for construction of a glucose biosensor. Biosens Bioelectron 2011;26:3456–3463.

[52] Robey RB, Hay N. Mitochondrial Hexokinases,N ovel mediators of the antiapoptotic effects of growth factors and Akt. Oncogene 2006;25:4683–4696.

[53] Shvedova AA, Castranova V, Kisin ER, Schwegler-Berry D, Murray AR, Gandelsman VZ, Maynard A, Baron P. Exposure to carbon nanotube material: assessment of nanotube cytotoxicity using human *Keratinocyte* cells. J Toxicol EnViron Health Part A 2003;66:1909–1926.

[54] Manna SK, Sarkar S, Barr J, Wise K, Barrera EV, Jejelowo O, Rice-Ficht AC, Ramesh GT. Single-walled carbon nanotube induces oxidative stress and activates nuclear transcription factor-κB in human Keratinocytes. Nano Lett 2005;5:1676–1684.

[55] Lam CW, James JT, McCluskey R, Hunter RL. Pulmonary toxicity of single-wall carbon nanotubes in mice 7 and 90 days after intractracheal instillation. Toxicol Sci 2004;77:126–134.

[56] Chen X, Tam UC, Czlapinski JL, Lee GS, Rabuka D, Zettl A, Bertozzi CR. Interfacing carbonn anotubes with living cells. J Am Chem Soc 2006;128:6292–6293.

[57] Kang S, Pinault M, Pfefferle L, Elimelech M. Single-walled carbon nanotubes exhibit strong antimicrobial activity. Langmuir 2007;23:8670–8673.

[58] Kang S, Herzberg M, Rodrigues DF, Elimelech M. Antibacterial effects of carbon nanotubes: size does matter! Langmuir 2008;24:6409–6413.

[59] Akhavan O, Abdolahad M, Abdi Y, Mohajerzadeh S. Silver nanoparticles within vertically aligned multi-wall carbon nanotubes with open tips for antibacterial purposes. J Mater Chem 2011;21:387–393.

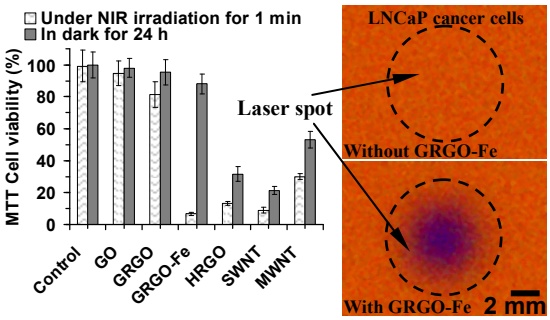

Photothermal cancer therapy using graphene oxide (GO) reduced by glucose in the presence of Fe (GRGO-Fe), hydrazine-reduced GO and CNTs.